Materials Science and Engineering C 67 (2016) 294–303

Contents lists available at ScienceDirect

Materials Science and Engineering C

journal homepage: www.elsevier.com/locate/msec

Surface chemistry of Ti6Al4V components fabricated using selective laser melting for biomedical applications

Jayasheelan Vaithilingam [a,*], Elisabetta Prina [b], Ruth D. Goodridge [a], Richard J.M. Hague [a], Steve Edmondson [c], Felicity R.A.J. Rose [b], Steven D.R. Christie [d]

[a] Additive Manufacturing and 3D Printing Research Group, EPSRC Centre for Innovative Manufacturing in Additive Manufacturing, School of Engineering, The University of Nottingham, Nottingham NG7 2RD, UK
[b] School of Pharmacy, Centre for Biomolecular Sciences, The University of Nottingham, Nottingham NG7 2RD, UK
[c] School of Materials, The University of Manchester, Manchester M13 9PL, UK
[d] Department of Chemistry, Loughborough University, Loughborough LE11 3TU, UK

ARTICLE INFO

Article history:
Received 21 December 2015
Received in revised form 27 April 2016
Accepted 12 May 2016
Available online 13 May 2016

Keywords:
Additive manufacturing
3D printing
Selective laser melting (SLM)
Surface chemistry
Ti6Al4V
Cytotoxicity

ABSTRACT

Selective laser melting (SLM) has previously been shown to be a viable method for fabricating biomedical implants; however, the surface chemistry of SLM fabricated parts is poorly understood. In this study, X-ray photoelectron spectroscopy (XPS) was used to determine the surface chemistries of (a) SLM as-fabricated (SLM-AF) Ti6Al4V and (b) SLM fabricated and mechanically polished (SLM-MP) Ti6Al4V samples and compared with (c) traditionally manufactured (forged) and mechanically polished Ti6Al4V samples. The SLM–AF surface was observed to be porous with an average surface roughness (Ra) of 17.6 ± 3.7 μm. The surface chemistry of the SLM-AF was significantly different to the FGD-MP surface with respect to elemental distribution and their existence on the outermost surface. Sintered particles on the SLM-AF surface were observed to affect depth profiling of the sample due to a shadowing effect during argon ion sputtering. Surface heterogeneity was observed for all three surfaces; however, vanadium was witnessed only on the mechanically polished (SLM-MP and FGD-MP) surfaces. The direct and indirect 3T3 cell cytotoxicity studies revealed that the cells were viable on the SLM fabricated Ti6Al4V parts. The varied surface chemistry of the SLM-AF and SLM-MP did not influence the cell behaviour.

1. Introduction

Additive manufacturing (AM) is attractive for fabricating biomedical implants due to its ability to fabricate customised parts with complex shapes [1]. Selective laser melting (SLM), a metal-based AM technique, enables the direct fabrication of parts from three dimensional (3D) model data by fusing metal powder particles together in a layer-by-layer method [2–4]. SLM not only has the ability to produce complex parts with desirable shape and structure but also has the advantage of establishing a closed process chain from scanning a damaged part of the body to design and manufacture. For example, bone replacement parts can be fabricated by scanning the bone defect using magnetic resonance imaging (MRI) or computer tomography (CT), designing the implant structure, then directly manufacturing the individual implant. This closed process chain has the potential to offer custom-fitting implants designed and produced specifically for the damaged part's anatomy [5]. Also the freedom of design offered by this technology enables the fabrication of implants with complex geometries, in terms of both external and internal morphology [5].

Previous studies on SLM have so far focussed on its ability to build complex structures, optimising processing conditions, mechanical properties, microstructural analysis and surface morphology [6–8]. There has also been research into biocompatibility and cell growth, proliferation and differentiation on SLM fabricated Ti6Al4V structures [9–11]. However, there is limited literature investigating the surface composition of Ti6Al4V parts fabricated using SLM. Since the powder is melted and cooled rapidly during the SLM process, there is the possibility for a SLM fabricated part to differ in its surface chemistry compared to a conventionally manufactured part (e.g. those made by casting, forging etc.). For example, it has been shown that segregation of Al can occur during SLM of Ti6Al4V due to rapid melting and cooling of the alloy [12]. Such segregation of alloying elements can potentially alter the surface chemistry of the alloy significantly by altering its surface oxide composition.

Typically, the surface chemistry of a part mainly depends on the distribution of its alloying elements on the surface and the atmosphere to which the part is exposed to. Inclusion and discontinuity spots that

* Corresponding author at: Additive Manufacturing and 3D Printing Research Group, School of Engineering, Coates Building, University Park, University of Nottingham, Nottingham NG7 2RD, UK.
E-mail address: Jayasheelan.Vaithilingam@nottingham.ac.uk (J. Vaithilingam).

http://dx.doi.org/10.1016/j.msec.2016.05.054

arise due to surface heterogeneity may affect biocompatibility [13]. For example, in the case of Ti6Al4V, aluminium or vanadium present on the surface may form their corresponding oxides and reduce the stability of the surface oxide layer which can lead to poor biocompatibility [14]. The presence of alloying elements on the implant surface can influence the dissolution of ions in the biological environment. Clinical experience has shown the release of vanadium ions from implants made of Ti6Al4V to the body [15]. These metal ions interfere with cell differentiation and contribute to periprosthetic osteolysis by impairing osteogenesis [16].

A biomaterial interacts with the biological environment at a bio-interface where biology meets the material. Bio-interphases are affected by the nature of the biomaterials including its surface energy, surface chemistry, surface morphology and surface roughness [17–19]. Without a good understanding of the surface chemistry, the interaction of cells at the interfaces will be poorly understood. Although several surface modification techniques such as passivation, chemical etching, ion-implantation etc., are available to improve and modify the surface chemistry of an implant [18–21], the principle source of those surfaces is the manufacturing process.

Biological reactions take place at the implant-host interface and hence the surface chemistry of the implant (in the first few nanometres) will play a significant role [1]. X-ray Photoelectron Spectroscopy (XPS) is a reliable tool in measuring the surface chemistries of a sample approximately for up to 10 nm. Therefore, in this study, XPS was used to determine the surface chemistries of (a) SLM as-fabricated (SLM-AF) Ti6Al4V and (b) SLM fabricated and mechanically polished (SLM-MP) Ti6Al4V samples and compared with (c) traditionally manufactured (forged) and mechanically polished (FGD-MP) Ti6Al4V samples. Previous studies have shown that SLM produced Ti6Al4V parts were biocompatible and favoured cell proliferation and growth [22–24]. In the present study, cytotoxicity of SLM fabricated samples (SLM-AF and SLM-MP) were evaluated and related to its surface chemistry.

2. Materials and methods

2.1. Materials

Ti6Al4V, a grade 5 titanium alloy plasma-atomised powder with an average particle size (volume weighted) of 33.35 μm, was supplied by LPW Technology Ltd., UK. Solvents including dichloromethane, methanol, ethanol and deionised water (supplied by Sigma-Aldrich, UK.) were used for cleaning the samples in a sonicator. Forged Ti6Al4V plate was purchased from TIMET UK Ltd., UK. Silicon carbide grits, polishing cloth and the extender solutions were supplied by Buehler (Buehler-met® II). Materials used for the cell tests are provided in cytotoxicity studies section.

2.2. Selective laser melting

Cuboidal Ti6Al4V components with dimensions of 10 × 10 × 3 mm (XYZ) were fabricated in a Renishaw AM 250. The machine is equipped with a fibre modulated pulse laser with a maximum power of 200 W and wavelength of 1070 nm. Previously optimised SLM process parameters used for the study are tabulated in Table 1. A multi-directional meander scan strategy was used where the laser scan direction was rotated by 67° for each layer to reduce the residual stress. The components were built on a Ti6Al4V metal substrate preheated to 80 °C. The build chamber was filled with argon gas to maintain an inert atmosphere. The initial residual oxygen level was 900 ppm and this reduced to 1 ppm in due course. The temperature of the build chamber during the process was 34–36 °C.

The SLM machine consisted of a hopper attached to a wiper, an elevator that lowered the substrate to adjust the layer thickness and a lens that focused the laser to the build area. The powder from which the part was to be fabricated was spread over the build platform from a hopper to the pre-defined layer thickness (50 μm). After the layer was spread, the laser beam scanned and fused the powder in the areas specified by the layer of the CAD file. Once the scan was complete, the elevator lowered by the pre-defined layer thickness for the powder to be spread for the next layer and this process continued until the part was completed. A detailed procedure for the SLM process and the parameters that govern SLM can be found in [25].

Table 1
SLM process parameters used to produce samples for surface characterisation.

Laser power	200 W
Hatch spacing	100 μm
Point distance	50 μm
Exposure time	220 μs
Layer thickness	50 μm
Scan strategy	Meander
Build plate temperature	80 °C

2.3. Sample preparation

A SLM fabricated and a hot forged Ti6Al4V sample were roughly polished using a series of silicon carbide grits (220 μm, 400 μm, 600 μm, 800 μm and 1200 μm diameter) for 5 min each in a polishing machine. The gritted samples were then polished using a polishing cloth with 6 μm and 1 μm diamond paste (3 min each). Three SLM-AF, SLM-MP and FGD-MP samples were sonicated separately in solvents including dichloromethane, methanol, ethanol and deionised water for 10 min each and dried using compressed air. Sonication was performed to remove any contaminants that might have been present on the surface of the samples and to remove any loosely bound Ti6Al4V particles from the SLM fabricated surface.

2.4. Surface characterisation

2.4.1. Scanning electron microscopy (SEM)

A LEO 440 SEM was used to obtain images of the surface morphology of the SLM fabricated Ti6Al4V plates. The SEM was operated at an extra-high voltage (EHT) power supply of 10 kV. Samples were mounted on an aluminium stub using carbon cement.

2.4.2. Surface profilometry

An Alicona InfiniteFocus® optical 3D measurement device was used to measure the surface roughness (Ra) of the SLM-AF, SLM-MP and FGD-MP Ti6Al4V components. A 175 μm × 175 μm square area was used to obtain the surface roughness pattern. The in-built software within the Alicona InfiniteFocus® surface profilometer was used to process the acquired data from the equipment.

2.4.3. X-ray photoelectron spectroscopy (XPS)

XPS measurements were performed using a Thermo Scientific K-Alpha ESCA with a probing spot size of 400 μm. Using aluminium (Al) Kα monochromated radiation at 1486.6 eV, photoelectrons were collected using a take of angle of 90°. In a constant analyser energy mode, survey spectra were collected at a pass energy of 100 eV and high resolution spectra were obtained at a pass energy of 20 eV. Depth profiles were obtained by sputtering the specimen at a rate of 1.35 Å/s using a 2 K eV argon ion gun. The relative intensity of the detected elements was plotted against binding energy and the chemical composition of the surface was characterised. Peak deconvolution was performed using Gaussian-Lorentzian curves to obtain the chemical states of the elements present in the surface. A built-in Thermo Scientific Avantage data system was used for data acquisition and processing. Previously reported works [26,27] and the National Institute of

Standards and Technology (NIST) database were used to identify the spectral lines. Statistical analysis of the XPS results was performed by analysing three areas of each SLM-AF, SLM-MP and FGD-MP sample. The equipment error due to calibration for this study was ±10% in addition to the reported mean ± standard deviation.

2.5. Cytotoxicity studies

To investigate the suitability of the SLM fabricated Ti6Al4V samples (SLM-AF and SLM-MP) for biomedical applications, cytotoxicity studies (indirect and direct) were performed. In the indirect study, the cell culture media that was in contact with the SLM fabricated surface was extracted and used to assess the cytotoxicity as a result of chemical leaching. In the direct study, the cells were grown directly on the SLM fabricated samples to evaluate the cell viability. For both the direct and indirect studies, immortalized NIH 3T3 mouse embryonic fibroblast cells (3T3 cells; passage number 50–53) grown in Dulbecco's Modified Eagle Medium (Gibco Life Technologies, UK) were used. The medium was supplemented with 10% (v/v) Foetal Bovine Serum (FBS), 2 mM L-glutamine (Sigma-Aldrich) and 1% (v/v) Gentamicin/Amphotericin B (Sigma-Aldrich, UK, 10,000 units ml-1 Penicillin, 10 mg ml^{-1} Streptomycin and 25 μg ml^{-1} Amphotericin B) at 37 °C, 5% CO_2 in air.

2.5.1. Indirect study

The SLM-AF and SLM-MP samples were sterilized with 70% (v/v) of isopropyl alcohol in water and dried under a laminar flow-hood overnight at room temperature. The samples were then rinsed with Phosphate Buffered Saline (PBS, Sigma-Aldrich) three times for 15 min. Cell culture media 800 μl, at a concentration of 1.25 cm^2/ml was added to each sample (SLM-AF and SLM-MP) and incubated at 37 °C, 5% CO_2 for 72 h to obtain the extract media. Cells were cultured to confluency at which point they were trypsinised and seeded into 96 well plate at a density of 100,000 cells/ml (100 μl) and incubated at 37 °C, 5% CO_2 in air. After 72 h, the media of each well was replaced with 100 μl of the extract media. The evaluation of the cytotoxicity of the samples was performed by quantifying the lactate dehydrogenase (LDH, Thermo Scientific) released from the cells after 24 h and 72 h, according to the manufacturer's protocols. Briefly, 50 μl of media was collected from each sample and mixed with a reaction mixture (0.6 ml of Assay Buffer with 11.4 ml of Substrate Mix in pure water) and incubated at room temperature for 30 min. Later, 50 μl of Stock solution was added to each well. The absorbance at 680 nm was measured using a Tecan Infinite M200 microplate reader and subtracted from the 490 nm absorbance. As a positive control, a maximum LDH activity was measured by adding 10 μl of lysin buffer (10×) to cells. As a negative control, LDH activity was measured in media taken from cells cultured in fresh media. The evaluation of the viability of 3T3s grown for 24 h and 72 h in the extract media was tested using the PrestoBlue® assay (Invitrogen) following manufacturers guidelines. Briefly, a 1:10 solution of PrestoBlue® was prepared in fresh culture media which was then added to the samples at the appropriate time point, and incubated at 37 °C, 5% CO_2 in air. After 45 min, fluorescence was measured at 560 nm (excitation) and 590 nm (emission) using a Tecan Infinite M200 microplate reader. The percentage viability was obtained as the ratio of sample fluorescence intensity to the mean of control fluorescence intensity.

2.5.2. Direct test

For the direct test, 3T3 cells were seeded directly onto the samples. The SLM-AF and SLM-MP samples were placed in a 24 well plate, sterilized as previously mentioned in the indirect study and placed in cell culture media for 3 days prior to commencing the test. A cell suspension of 80,000 cells/ml was prepared and an aliquot of 1 ml was added to each sample. After 24 h, the samples were shifted to a new well plate and the metabolic activity of the attached cells was tested at day 1, 5 and 7 with a PrestoBlue® assay, as described for the indirect study. For each condition, the fluorescent intensity of a blank control (no cells) was subtracted from the sample readings. After each time period, 1 ml of fresh media was added to each sample and the samples then returned to the incubator. After 7 days, LIVE/DEAD® Viability/Cytotoxicity Assay Kit (Invitrogen) was used for a qualitative evaluation of live and dead cells seeded on the scaffolds. Cells on the samples were stained with 0.8 μM of Calcein AM and 1.6 μM of ethidium homodimer (EthD-1) and incubated at 37 °C, 5% CO_2 for 30 min. Fluorescence images were obtained using a Nikon SMZ1500 Stereoscopic Zoom Microscope and a Nikon digital sight DS-Fi2 camera.

2.6. Statistical analysis

For the cytotoxicity test, mean ± standard deviation is reported for five samples for a single experiment. Significance was assessed using Prism 6 software (GraphPad, v6.01) by Two-way ANOVA followed by a Bonferroni post-hoc test to compare groups. A value of $p < 0.05$ was considered significant.

3. Results

3.1. Surface morphology and roughness

Fig. 1 shows the surface morphology of the SLM-AF surface at various magnifications. From the micrograph it is can be seen that loosely bound and partially sintered particles were present on the surface. The observed surface roughness (Ra) using a surface profilometer was 17.6 ± 3.7 μm. The presence of partially melted particles on the part surface is inevitable in SLM, with the magnitude of this problem being dependent on both material and process parameters. Some of the parameters that influence the surface roughness of SLM fabricated parts are material, powder particle size, layer thickness, laser type and power, scan parameters and scan strategy [28,29].

3.2. Surface chemistry

Fig. 2 shows the survey spectra of the detected elements for SLM-AF, SLM-MP and FGD-MP confirming that the elements C, N, O, Ti and Al are present in all three samples. A week signal (≥0.3%) for vanadium was observed on the mechanically polished samples (SLM-MP and FGD-MP) and not on the SLM-AF. Since the SLM-AF samples were rough, this would have reduced the signal by reducing the electron counts

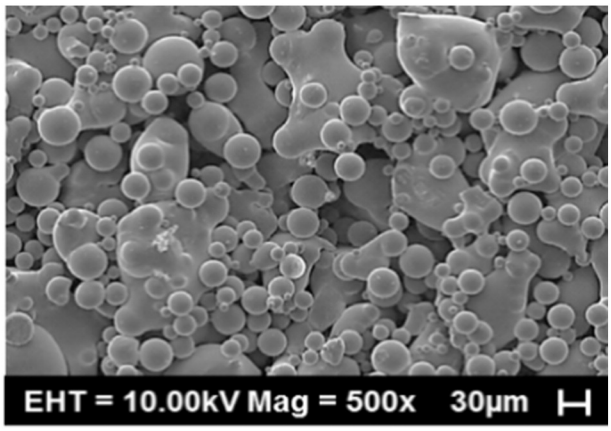

Fig. 1. SEM image showing the surface morphology of an as-fabricated Ti6Al4V surface fabricated using SLM. The figure clearly depicts the rough and porous nature of the SLM-AF surface.

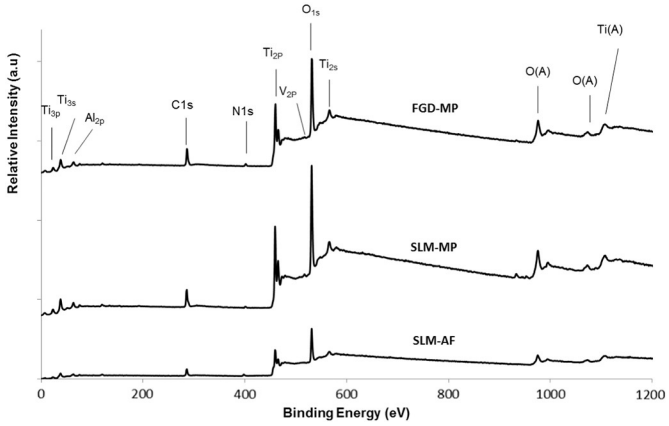

Fig. 2. Survey spectra of SLM as-fabricated (SLM-AF), SLM mechanically polished (SLM-MP) and forged mechanically polished (FGD-MP) Ti6Al4V surface.

reaching the detector during XPS characterisation and hence showing no vanadium on the SLM-AF surface.

Table 2 shows the relative atomic percentages of the detected elements. As can be observed from the table, the dominant signals of the spectra for all three samples are Ti, O and C with a weak contribution from Al and N. The ratios of Ti:O observed for SLM-AF (0.33), SLM-MP (0.26) and FGD-MP (0.27) were higher than the Al:O (0.13; 0.1 and 0.06 for SLM-AF, SLM-MP and FGD-MP) ratio. This revealed that the surface film of all three samples mainly composed of titanium oxide. To investigate the surface chemistry in detail and to determine the oxidation states of alloying elements, high resolution spectra of C, O, Al, Ti and V on the SLM-AF, SLM-MP and FGD-MP samples were obtained. Depth profiling was also performed to investigate the distribution on the detected elements and their chemical states in the first few nanometres of the Ti6Al4V components.

3.3. Depth profiling

Fig. 3 shows the high resolution spectra and depth profiling spectra of C and O for all three samples (SLM-AF, SLM-MP and FGD-MP). Before argon ion sputtering the sample, the deconvoluted C 1s peak showed the existence of metal carbide (281.7 ± 0.4 eV), C—C (285 eV) and C—O (288.9 ± 0.3 eV) bonds in all three samples [26]. Since Ti6Al4V is an alloy of Ti, Al and V, the metal carbide may have contributions from all three metals. However, since Ti is highly reactive, most of the observed metal carbide may have been from TiC. After sputtering the samples for 30 s (~4 nm), SLM-AF showed a reduction in the intensity of the C—C and C—O peaks whereas in SLM-MP and FGD-MP samples, the C—C and C—O peaks disappeared. The C—Ti peak was witnessed even after ion sputtering, for all three samples. The reduction in the carbon (C—C and C—O) after sputtering is likely to be due to the fact that most of the carbon was present on the surface as a contaminant. The slower decrease in C for the SLM-AF sample might be due to the rough nature of the SLM-AF surface. On depth profiling the sample, only the C—Ti was observed. Thus, depth profiling of the sample provided a powerful way to separate out the carbon contribution from atmospheric contamination. Also, ion sputtering the metal surface for a few (~5) nanometres will remove the adventitious carbon present on the surface.

On deconvolution of the high resolution O 1s spectra, peaks were observed at 530.2 ± 0.2 eV and 532.3 ± 0.4 eV (Fig. 3). The initial peak is due to the Ti—O and the peak observed at 532.3 ± 0.4 eV may be due to C═O, aluminium oxide and adsorbed water molecules [26]. The presence of adsorbed H_2O molecules could be due to the final cleaning procedure (using deionised water) or from atmospheric moisture. The Ti—O bond is due to the thin TiO film formed on the surface and C═O may be due to the contamination of surface with carbon containing molecules [27]. From the depth profiles, the concentration of O—Ti can be observed to decrease rapidly with depth for the SLM-MP and FGD-MP samples while it reduces slowly for the SLM-AF. The possible reasons for this sudden and slow drop of oxygen concentration are discussed Section 4.

Fig. 4 shows the high resolution Ti 2p, Al 2p and V 2p spectra and its evolution on depth profiling. A characteristic doublet peak shape and position observed at 459.1 ± 0.3 and 465.5 ± 0.4 eV for all three samples showed that Ti is mainly present on the surface as Ti^{4+} [27]. Hence, it is evident that the surface of the samples is dominated by TiO_2. Minor fractions of its sub-oxides Ti_2O_3 (457.8 ± 0.4 and 464.2 ± 0.2) and TiO (455.1 ± 0.3 eV and 460.9 ± 0.2 eV) were observed from the intensity of Ti 2P peak revealing their presence in the metal-oxide interface [26]. A small contribution from the Ti 2p metal (453.8 ± 0.2 eV and 460.1 ± 0.3 eV) was witnessed and this is due to the fact that the oxide is thinner than the electron escape depth [27]. On depth profiling of the samples, a clear shift of the TiO_2 peak to pure Ti metal doublet peak at 454.5 ± 0.2 eV and 460.6 ± 0.4 eV could be witnessed (Fig. 4). This confirms that TiO was only present in the first few nanometres.

The spectrum obtained for Al in the Al_{2P} region shows the possibility for the presence of Al both in its metallic and oxide form for all three samples (Fig. 4). Peaks observed at 71.8 ± 0.2 revealed the presence of metallic aluminium from the underlying bulk metal alloy and 74.6 ± 0.4 showed the presence of Al_{2P3} in the sapphire form of Al^{3+} (Al_2O_3) [26]. Also this Al^{3+} ion may exist as interstitial or substitutional ions in the TiO_2 matrix [26]. Similar to the Ti 2p peak, on depth profiling, an increase in the metallic Al and a decrease in its oxide form was observed for all three samples. However, the SLM-MP and FGD-MP showed a sudden shift from the oxide form to metallic Al whereas SLM-AF witnessed a slower change. This shows the transformation of Al^{3+} ion to metallic Al on depth profiling.

From Fig. 4, it can be observed that there is no V on the SLM-AF surface whereas it is observed on the SLM-MP and FGD-MP surfaces in low concentration. This could be due to the fact that the SLM-AF surface has comparatively higher Ti and Al concentration than the V concentration. With this very low concentration, the signals generated would be very low and this might have also been affected by the rough nature of the surface. Although V was not observed on the SLM-AF surface, after mechanical polishing, the alloying element is exposed to the atmosphere form its corresponding oxides (V_2O_3 and V_2O_5).

From Fig. 4, the deconvoluted V 2p peak shows the existence of V on the mechanically polished SLM-MP and FGD-MP surfaces. However, the concentration of V on the SLM-MP was lower than the concentration of

Table 2
Relative atomic percentage of elements detected using XPS for SLM-AF, SLM-MP and FGD-MP samples. Instrumental error due to calibration was approximated to ± 10%.

	Relative atomic percentage					
Sample type	Al 2p	C 1s	N 1s	O 1s	Ti 2p	V 2p
SLM-AF	5.4 ± 0.9	25.8 ± 3.6	3.2 ± 1.4	49.8 ± 2.8	15.8 ± 1.6	0
SLM-MP	6.0 ± 1.1	17.2 ± 4.6	1.2 ± 0.8	59.1 ± 3.7	16.1 ± 0.9	0.4 ± 0.2
FGD-MP	3.0 ± 1.5	32.6 ± 3.9	1.8 ± 0.5	49.2 ± 2.4	13.2 ± 2.0	0.3 ± 0.3

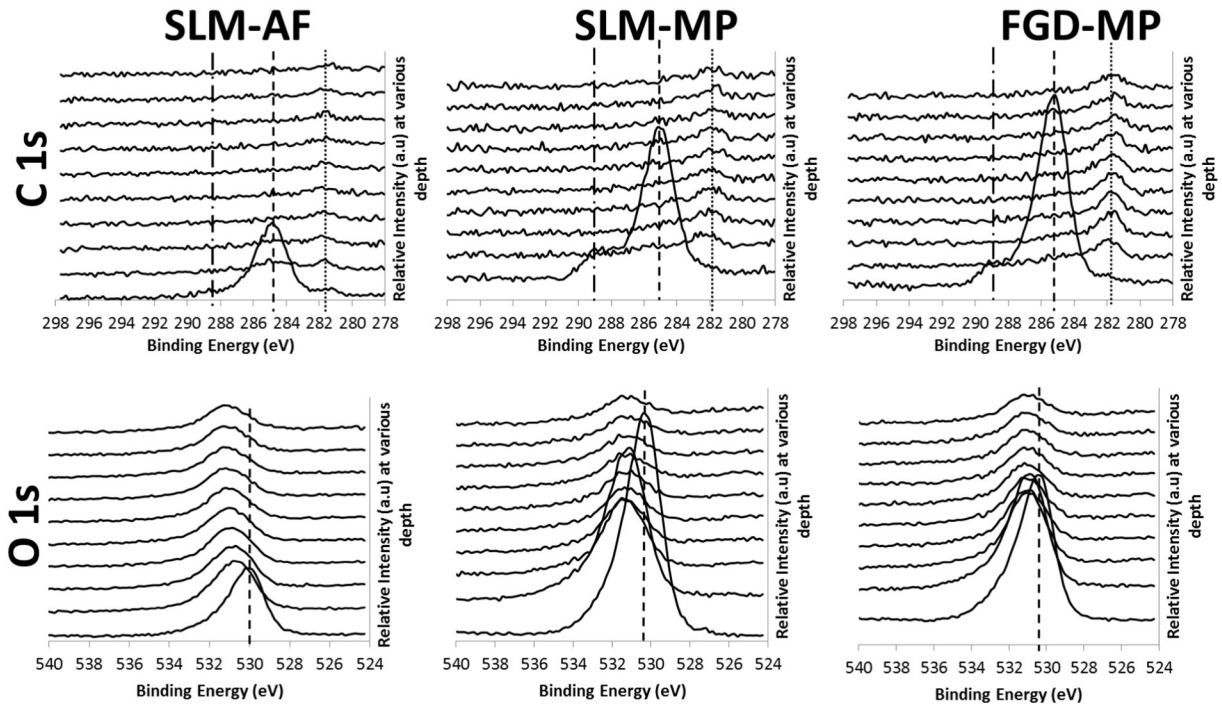

Fig. 3. Depth profile spectra of C 1s and O 1s regions for SLM-AF, SLM-MP and FGD-MP samples. Depth profiling was performed at every 30 s (~4 nm depth) from 0 to 270 s. C 1s spectra show the disappearance of the initially observed peak after 30 s of argon ion sputtering which is attributed to surface contamination. Reduction in the intensity of O 1s peak on increasing depth can also be witnessed from the figure.

V on FGD-MP. However, most of the V observed on the surface was recorded to be in its oxide form (V_2O_3 and V_2O_5) at 514.7 ± 0.3 eV and 516.8 ± 0.5 eV for both SLM-MP and FGD-MP. On depth profiling, XPS detected V in the SLM-AF sample (after sputtering ~4 nm) and the concentration of metallic vanadium (512 ± 0.2 eV) could be observed to increase for all three samples as a function of sputtering time.

3.4. Estimation of oxide layer thickness

Fig. 5 shows the graphical representation of the elemental distribution observed for SLM-AF, SLM-MP and FGD-MP samples. The thickness of the oxide film was estimated by two methods. In method 1, the thickness was calculated from the depth at which the oxygen content decreased to half of its maximum value during depth profiling. In method 2, the thickness was estimated from the depth at which the major alloying element Ti intersects the O in the depth profile. Since the SLM-AF was rough, a slow decrease in the oxygen concentration was observed. As a result, by method 1, the thickness of its oxide layer was observed to be >35 nm for SLM-AF and, 9.5 nm for SLM-MP and 15 nm for FGD-MP. For the second method, the observed thickness was approximately 15 nm for SLM-AF and ~6–7 nm for SLM-MP and FGD-MP samples. These measured oxide layer thicknesses for the polished samples were nearly consistent with literature showing an oxide layer of 1–10 nm [30]. From both methods, the oxide layer of the SLM-AF is almost double that of the mechanically polished SLM-MP and FGD-MP samples.

3.5. Cytotoxicity studies

The cell cytotoxicity due to chemicals leached from the SLM-AF and SLM-MP samples obtained from the indirect study (LDH and PrestoBlue® assay) are shown in Fig. 6.

The LDH assay indicates the cytotoxicity of the media and the PrestoBlue® assay indicates the metabolic activities of cells in contact with extract media. For both the SLM-AF and SLM-MP samples, after 24 h and 72 h, the LDH (Fig. 6a) released from the cells in contact with the extract media was comparable to the negative, or non-cytotoxic, control, and it was statistically different from the positive control. Fig. 6b demonstrates that 3T3 cells present a high viability with no significant difference between SLM-AF and SLM-MP in each time point (24 h and 72 h) considered.

The results of the metabolic activities of 3T3s seeded directly on the SLM-AF and SLM-MP samples are presented in Fig. 7. It can be observed that the fluorescence intensity significantly increased from day 1 (2225.4 ± 441.8, 1661.0 ± 205.0) to day 5 (21,117.8 ± 1777.6, 20,830.0 ± 2190.3) and day 7 (25,456.4 ± 1364.5, 28,179.6 ± 1522.6) for SLM-AF and SLM-MP, suggesting that the cells were viable and proliferated on both samples. Fig. 7A represents cells stained with Calcein AM and EthD-1. The majority of cells are green labelled indicating their high viability and the confluent cell layer confirms the high result of the fluorescence intensity obtained with the PrestoBlue assay. The black areas in Fig 7b for the SLM-AF sample were due to its porous nature.

4. Discussion

As noted in previous literature, the rough nature of the SLM-AF surface is due to the partial sintering of particles [29]. On mechanical polishing of the as-fabricated part, these partially sintered particles can be removed from the surface. The partially sintered particles will add to the thickness of the part thus increasing its wall thickness and surface area. The rough and porous nature of the SLM-AF is likely to affect the XPS measurement.

An important parameter to consider while estimating the oxide film thickness would be sensitivity of XPS to rough surfaces. During the measurement, the number of counts obtained for a rough surface (SLM-AF) was considerably lower than the counts obtained for a polished surface (SLM-MP and FGD-MP). Since the surface is highly porous and uneven

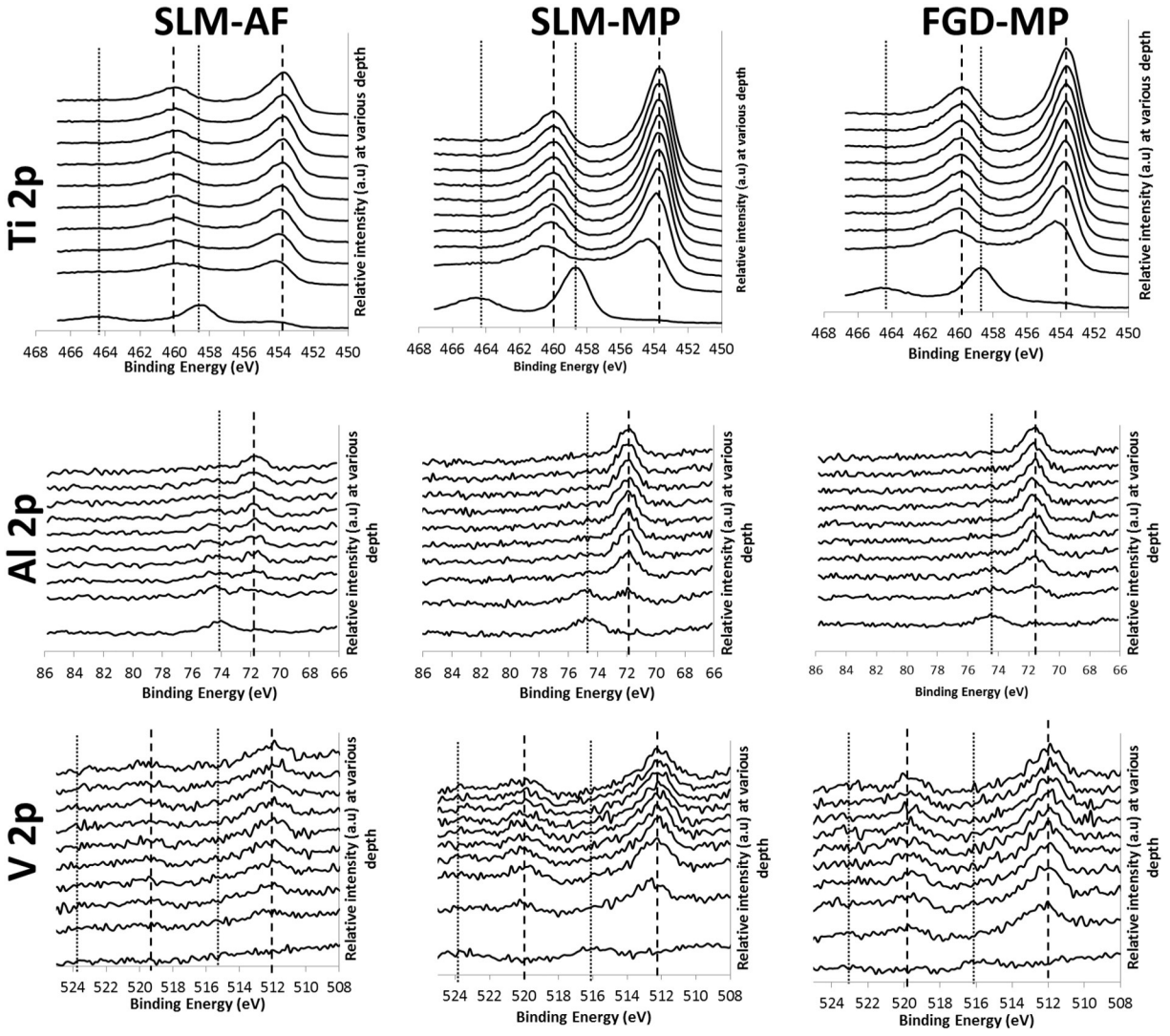

Fig. 4. Depth profiles of Ti 2p, Al 2p and V 2p for SLM-AF, SLM-MP and FGD-MP samples. A clear transformation of oxide to pure metal on depth profiling can be witnessed for all three metals.

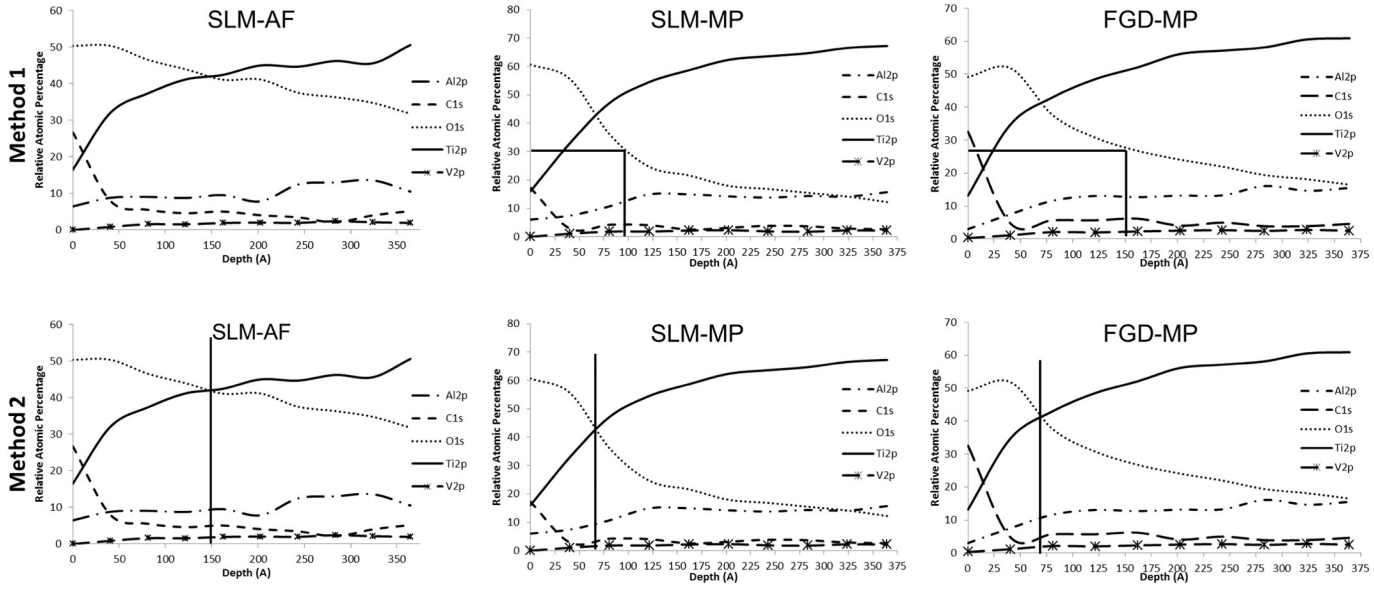

Fig. 5. Estimation of oxide layer thickness for SLM-AF, SLM-MP and FGD-MP samples using two different methods. Data points at every 30 s of ion sputtering (~4 nm depth).

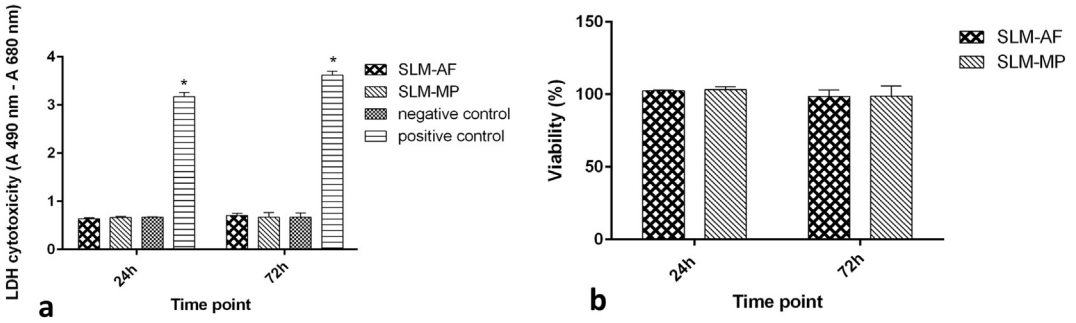

Fig. 6. Indirect cytotoxicity studies. (a) LHD activities after 24 h and 72 h. SLM-AF and SLM-MP (a) are comparable to the negative control ($p < 0.05$). The (*) symbol represent statistical difference between positive control and other condition ($p < 0.05$) at each time point. (b) Cell viability (%) measured after 24 h and 72 h of 3T3 cultured in extract media compared to the control. No statistically significant differences were observed between SLM-AF and SLM-MP for the time points considered.

due to sintered particles, this gives varied incident angles for the XPS beam (see Fig. 8). Hence, the number of electrons that pass through the analyser will be significantly lower when compared to a polished surface. When the surface morphology is uneven, it is difficult to sputter the surface equally due to a shadowing effect. As a result, some elements present on the outermost surface can still be detected even in a deeper location in the depth profile. Due to this shadowing effect and uneven ion sputtering of the sample surface, the SLM-AF samples showed a gradual change in its detected elemental composition.

Together with the major alloying elements Ti, Al and V, XPS detected C, O and N. Bulk metals react with air and form their corresponding oxides, carbides and nitrides depending on the atmospheric conditions [27]. Although the SLM process is carried out in an argon atmosphere with oxygen concentration <1 ppm, there is the possibility of titanium reacting with the available oxygen and forming its oxide. Also, there is no control of the carbon dioxide during the SLM process and the amount of carbon present in the build atmosphere/chamber remains unknown. Although Ti6Al4V has 0.08% (max) carbon in its composition, a considerable amount of carbon is also present in the powder itself due to atmospheric contamination.

XPS detected C—C, C—O and C═O bonds can be due to hydrocarbons from air, manual handling, solvents used for cleaning purposes [27,31]. Since solvents including dichloromethane, methanol and ethanol were used for cleaning purposes, these solvents may have left behind residues that were not washed away by deionised water. Also, there is the possibility for contamination due to adventitious carbon in the atmosphere while mounting and transferring the sample into the XPS machine [32]. On sputtering the surface, the concentration of carbon decreased significantly in the first few nanometres suggesting that they are mainly from contamination. However, a small amount of C was observed for all three samples at 281.7 ± 0.4 eV that corresponds to titanium carbide. Formation of this titanium carbide (TiC) may be during the manufacturing process itself. Due to the higher reactivity of Ti, it may readily react with carbon from CO_2 to form carbide. An exothermic formation of oxides and carbides of Ti during SLM process was previously reported to play a significant role in the instability of the melt pool [33].

The survey spectra showed the presence of N on all three samples (Fig. 2). Previous studies have shown that the contribution to the nitrogen peak can be from organically and inorganically bound N. Inorganically bound N can originate from a small amount of TiN_x in the surface film since titanium readily reacts with nitrogen. Organically bound nitrogen could be from organic contaminants such as proteins from manual handling or the atmosphere [27].

Although the build chamber was inerted with argon, the obtained results for SLM-AF and SLM-MP showed the formation of metal carbides and nitrides during laser processing. It is thought that this is due to the chemical reaction of the Ti and Al with the carbon and nitrogen in the build chamber. Formation of metal carbides/nitrides may potentially affect the wettability which in turn can affect the quality of the manufactured part. Hence the presence of carbon and nitrogen in the build chamber should be controlled. However, existence of metal carbide was also witnessed for the FGD-MP surface.

All three surfaces were observed to have TiO_2 as a surface film. Due to the presence of Al^{3+} ions on all three surfaces, it is likely that the surfaces also contain Al_2O_3 [26,27,34]. However, the implied concentration of Al_2O_3 on all these surfaces was lower than the implied concentration of TiO_2. Vanadium was not observed on the SLM-AF whereas SLM-MP

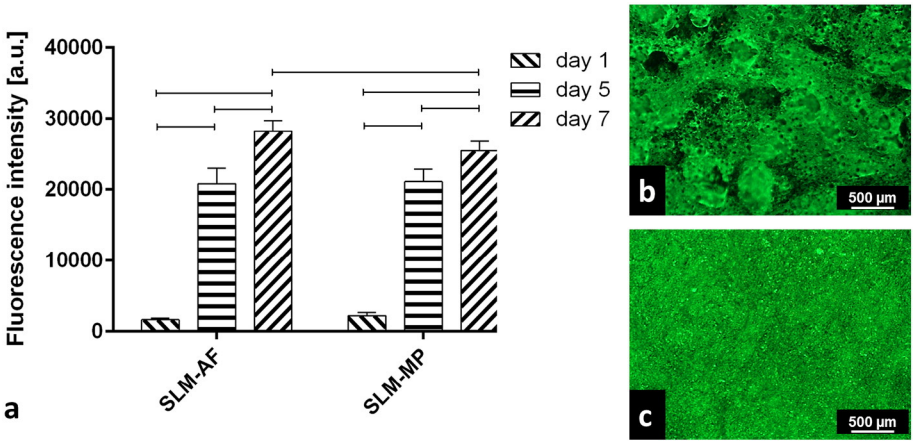

Fig. 7. Direct cytotoxicity studies. (a) Metabolic activities of cells seeded on SLM-AF and SLM-MP materials after 1 day, 5 day and 7 days. Statistically significant differences ($p < 0.05$) were found between day 1, day 5 and day 7 for both materials. Fluorescence images of cells seeded on the (b) SLM-AF and (c) SLM-MP stained with Calcein-AM (green represents live cells) and Ethidium homodimer (red represents dead cells) after 7 days. (For interpretation of the references to colour in this figure legend, the reader is referred to the web version of this article.)

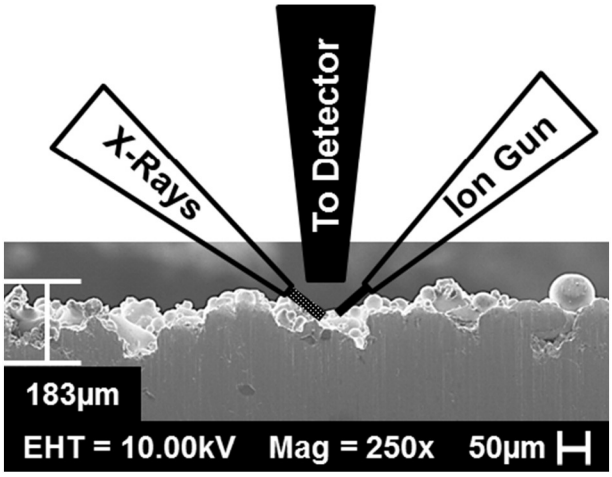

Fig. 8. Schematic of XPS probing on a rough SLM-AF Ti6Al4V component.

and FGD-MP surfaces were observed to have vanadium on their surface as V_2O_3 and V_2O_5. However, the concentration of vanadium is low in both SLM-MP (0.3%) and FGD-MP (0.4%). When the concentration of an element is lower than 0.3%, XPS will struggle to detect that particular element. Similarly in SLM-AF, the concentration of V might have been too low that XPS could not detect it. Another possible reason for the non-existence of V in SLM-AF is the oxide layer on the SLM-AF is formed during the process and it is dominated by Ti and Al. In contrast, the oxide layer on the SLM-MP and FGD-MP is formed after mechanical polishing. During mechanical polishing of the Ti6Al4V samples, the first few micron layers of the material are removed. As a result, Ti, Al and V are exposed to the atmosphere which leads to the formation of its corresponding oxides. Hence the concentration of V on the surface might have increased and XPS was able to detect it. A previous study revealed that recycling of Ti6Al4V powders increased the thickness of its surface oxide layer [37].

Ti has a high affinity towards O and moreover O has high solubility in Ti [34]. When Ti is exposed to O, it forms a monolayer of oxygen on the metal surface. The oxide is then formed by the diffusion of O atoms into the metal and/or metal ion diffusion on to the surface. After nucleation, the oxide grows laterally to cover the whole surface [34]. This reaction continues until the diffusion of O ceases leading to the formation of a passive oxide film. Since the SLM-AF surface is highly porous and in some areas porous beyond the surface, it is possible that there is a greater chance for more oxygen to diffuse into the metal and increase the oxide layer thickness. The structure of the oxide layer (amorphous or crystalline) is entirely dependent on the environment. To form a well-ordered crystalline structure, controlled environment is required [35]. During SLM, the Ti6Al4V is melted and solidified rapidly by the laser. Pequegnat et al. [36] reported amorphous TiO_2 for the laser processed Ti alloy with a possibility for a small fraction of crystallinity (anatase). Hence, the TiO_2 layers are expected to be in amorphous form with some degree of crystallinity.

SLM-AF sample was observed to have a thick oxide layer of almost double that of the mechanically polished samples. The values obtained for SLM-AF using method 1 showed the presence of a thick oxide layer (>35 nm). In the SLM process, parts are built layer-by-layer and this means that every layer will be exposed to the atmosphere within the build chamber for few seconds until a fresh layer is laid. Although argon gas is used to inert the SLM process chamber, there is still the possibility for the presence of oxygen at a very small concentration (<8 ppm). This oxygen may react with the laser scanned area to saturate the layer whereas this may not be the case in forging. Hence the process conditions might be a reason for the formation of thick oxide on the SLM fabricated samples. However, the gradual change in the elemental composition of Ti and O compared to the mechanically polished surfaces (SLM-MP and SLM-AF) during depth profiling shows that XPS characterisation of the sample was affected by the rough nature of the SLM-AF surface. Thus, the oxide layer thickness of SLM-AF was observed to be higher than mechanically polished surfaces.

On comparing the oxide layer thickness for the mechanically polished samples using method 1, FGD-MP appeared to show a thicker oxide layer (~15 nm) than SLM-MP (~10 nm). Although this may be true, one of the reasons for this might have been the effect of high carbon contamination observed on the FGD-MP surface. The carbon contaminant present above the surface oxide layer might have initially masked a certain concentration of the oxygen. This masking effect can be clearly observed from the depth profiling of FGD-MP (an increase in the oxygen concentration as carbon concentration drops). Thus depth profiling of a metal sample's surface renders useful information to examine if the carbon present on the surface is due to contamination or from its alloy.

In method 2, SLM-MP and FGD-MP showed similar thickness values (~6.5 nm and ~7 nm) which were lower than SLM-AF (~15 nm). Since these SLM-MP and FGD-MP samples were mechanically polished, the oxide layer formed may not be representative of the true oxide layer formed during the manufacturing process. Also, due to mechanical polishing of the samples, there will be no or a very minimal shadowing effect caused due to partially sintered particles during ion sputtering and hence their values are closer.

The presence of loosely bound and partially sintered particles can cause acute and/or chronic effects if they peel-off from the surface when implanted. Hence chemical etching of implants is required. Although etching of implants would be useful to remove the partially sintered particles, etching of Ti6Al4V using a strong oxidising agent such as piranha solution or a mixture of hydrofluoric acid and nitric acid will strip-off the native oxide layer formed during the manufacturing process. Titanium has the tendency to readily form oxide when exposed to air or water molecules to regenerate a fresh oxide layer [38]. During etching, micro-rough surfaces are produced and as a result, oxygen will penetrate into the bulk through these micro-pits and will form a thick oxide layer [39]. However, depending on the etchant and etching time, the thickness of the surface oxide layer will vary significantly. Typically, the thickness of the surface oxide layer can be increased by chemical etching [26]. If the increase in the surface oxide layer is above 10 nm and vanadium was not one of the contributing oxides, then it may not be possible for XPS to detect the vanadium from the sample.

"In addition to XPS, chemical analysis using energy dispersive x-rays (EDX), auger electron spectroscopy, grazing angle x-ray diffraction and time-of-flight secondary ion mass spectrometry (TOF-SIMS) are some of the commonly used equipment to characterise the surface chemical composition. However, as mentioned before, surface chemical measurements using almost all of these are affected by the surface roughness of the sample. Etching of a sample using an ion beam in a circular path rather than etching at a fixed angle can possibly minimise the shadowing effect caused by the rough surface. XPS is widely considered as a reliable tool in measuring the surface chemistry for up to 10 nm. By peak fitting the curve, it gives an indication of the possible bonding with other elements. This will enable a better understanding of the surface chemical compositions and its electronic states. Hence in order to understand the surface chemical composition, its electronic states and the bonding with other elements, XPS was used".

The indirect 3T3 cell-cytotoxicity was performed to observe any possible dissolution of metal ions to the culture medium and its impact on the cell behaviour. The indirect study revealed that the cells were viable when cultured on both SLM-AF and SLM-MP samples for the 7 day study period. This demonstrates that there was almost no dissolution of metal ions from both the SLM-AF and SLM-MP samples to the culture medium. The direct 3T3 cell study revealed that the cells were viable on both surfaces and there was no significant difference between them. The fluorescence intensity (due to cells) was observed to increase with the increase in the study time period showing good cell adhesion, growth

and proliferation. Thus both the direct and indirect cell studies demonstrate that the difference in the surface chemistry of these SLM-AF and SLM-MP did not influence the cell viability/growth over the studied 7 day time period.

Although the varied surface chemistry did not have a significant impact on the cellular response for this short time period, prolonged use of the material can possibly have a varied cellular response. The presence of aluminium oxide in the oxide film can affect the stability of the oxide layer and can potentially lead to the dissolution of metal ions into the biological environment when implanted for a longer period. In addition, an oxidised alloy surface will react differently to oxidised commercially pure Ti. They may react either directly by interacting with biomolecules or indirectly via corrosion behaviour (due to the presence of heterogeneous oxides) [27]. The absence of vanadium on the SLM-AF surface may be beneficial; however, if the partially sintered particles peel-off from the surface it may lead to acute or chronic effects. Also, highly porous surfaces are easily contaminated and sterilisation of such surfaces may be difficult. Vanadium observed on the mechanically polished surfaces may impose a serious threat on dissolution since it is not biocompatible. Due to this surface heterogeneity in both the SLM-AF and SLM-MP Ti6Al4Vsamples, adoption of a suitable surface modification technique may be required to form a homogenous surface and enhance the biocompatibility of the SLM fabricated surface.

Surface treatments including mechanical polishing, chemical etching, heat treatment, laser processing, electropolishing and anodisation can significantly alter the corrosion resistance of an implant [36,40]. For example, by anodising an implant surface, oxide layer thickness of >100 nm is possible thereby increasing the corrosion resistance [41]. It is difficult to give a definitive layer thickness to ensure the protection of Ti6Al4V implants in the biological environment. This would depend on various factors including the implanted location, concentration and type of ions in the biological environment and the surface elemental composition of the implanted material. However, thick surface oxide layer has the possibility to improve the corrosion resistance [38]. Other surface modifications such as growing multiple layers of proteins (such as laminin and fibronectin) [42] found in the body, functionalising the surface by chemically binding bioactive materials [43], coating biocompatible materials such as hydroxyapatite, calcium phosphates [19], polycaprolactone [44] will prevent the implant being exposed to the biological environment. As a result, release of harmful metal ions can be controlled.

5. Conclusions

- The ratio of Ti:Al suggests that the SLM-MP (2.68) has a relatively high aluminium on the surface than the SLM-AF (2.93) and FGD-MP (4.4) with FGD-MP having the lowest concentration.
- The thickness of the surface oxide layer by both methods were in the order of SLM-AF > FGD-MP > SLM-MP. The surface oxide layer thickness of the SLM-AF was double that of the SLM-MP and FGD-MP samples. However, the oxide layer thickness of the SLM-AF might have been partly influenced by the rough nature of the surface.
- The surface oxide film of SLM-AF was mainly composed of oxides of Ti and Al, whereas the surface oxide film of the SLM-MP and FGD-MP samples was composed of Ti, Al and V. Due to this surface heterogeneity, surface modification is required to achieve a uniform surface chemistry for medical applications.
- Depth profiling confirmed that most of the carbon and nitrogen observed on all three surfaces (SLM-AF, SLM-MP and FGD-MP) was from contamination. However Carbides and nitrides of titanium were observed to be formed during the SLM process by reacting with the available carbon and nitrogen in the build atmosphere.
- Both the direct and indirect 3T3 cell studies showed that the cells were viable on both the SLM-AF and SLM-MP surfaces without any significant difference. This reveals that there was almost no dissolution of metal ions to the cell/culture medium for the studied 7 day time interval. Thus, the SLM fabricated Ti6Al4V samples are suitable for short term biomedical applications.

Acknowledgement

This work was supported by the Engineering and Physical Sciences Research Council (EPSRC; UK) under grant EP/I033335/2 and the Medical Research Council (MRC)-EPSRC Centre for Doctoral Training (CDT) in Regenerative Medicine (EP/L015072/1; studentship awarded to E. Prina).

References

[1] J. Vaithilingam, R. Goodridge, S.D.R. Christie, S. Edmondson, R.J.M. Hague, Additive manufacturing and surface modification of biomaterials using self-assembled monolayers, in: H. DE, W. Chrzanowski (Eds.), Biointerfaces Where Material Meets Biol, first ed.Royal Society of Chemistry 2015, pp. 30–54.
[2] J. Kruth, B. Vandenbroucke, J.V. Vaerenbergh, I. Naert, Rapid manufacturing of dental prostheses by means of selective laser sintering/melting, J. Dent. Technol. 2 (2007) 24–32.
[3] I. Drstvensek, N.I. Hren, T. Strojnik, T. Brajlih, B. Valentan, Applications of rapid prototyping in cranio-maxilofacial surgery procedures, Int. J. Biol. Biomed. Eng. 2 (1) (2008) 29–38.
[4] R. Bibb, D. Eggbeer, P. Evans, Rapid prototyping technologies in soft tissue facial prosthetics: current state of the art, Rapid Prototyp. J. 16 (2) (2010) 130–137.
[5] M. Lindner, S. Hoeges, W. Meiners, K. Wissenbach, R. Smeets, R. Telle, et al., Manufacturing of individual biodegradable bone substitute implants using selective laser melting technique, J. Biomed. Mater. Res-A. 97 (4) (2011) 466–471.
[6] J. Kruth, M. Badrossamay, E. Yasa, J. Deckers, L. Thijs, J.V. Humbeeck, Part and material properties in selective laser melting of metals, 16th International Symposium on Electromachining 2010, pp. 1–12.
[7] I. Yadroitsev, A. Gusarov, I. Yadroitsava, I. Smurov, Single track formation in selective laser melting of metal powders, J. Mater. Process. Technol. 210 (12) (2010) 1624–1631.
[8] I. Yadroitsev, L. Thivillon, P. Bertrand, I. Smurov, Strategy of manufacturing components with designed internal structure by selective laser melting of metallic powder, Appl. Surf. Sci. 254 (4) (2007) 980–983.
[9] P.H. Warnke, T. Douglas, P. Wollny, E. Sherry, M. Steiner, S. Galonska, et al., Rapid prototyping : porous titanium alloy scaffolds produced by selective laser melting for bone tissue engineering, Tissue Eng. Part C. 15 (2) (2009) 115–124.
[10] A. Fukuda, M. Takemoto, T. Saito, S. Fujibayashi, M. Neo, D.K. Pattanayak, et al., Osteoinduction of porous Ti implants with a channel structure fabricated by selective laser melting, Acta Biomater. 7 (5) (2011) 2327–2336.
[11] D.K. Pattanayak, A. Fukuda, T. Matsushita, M. Takemoto, S. Fujibayashi, K. Sasaki, et al., Bioactive Ti metal analogous to human cancellous bone : fabrication by selective laser melting and chemical treatments, Acta Biomater. 7 (3) (2011) 1398–1406.
[12] J. Kruth, B. Vandenbroucke, J. Van Vaerenbergh, P. Mercelis, Benchmarking of different SLS/SLM processes as rapid manufacturing techniques, International Conference on Polymers and Moulds Innovations 2005, pp. 1–7.
[13] T. Hryniewicz, R. Rokicki, K. Rokosz, in: R. Pignatello (Ed.), Magnetoelectropolished titanium biomaterial 2011, pp. 227–247 Biomater. Sci. Eng. First edit. INTECH.
[14] B.O. Aronsson, J. Lausmaa, B. Kasemo, Glow discharge plasma treatment for surface cleaning and modification of metallic biomaterials, J. Biomed. Mater. Res. 35 (1) (1997) 49–73.
[15] J. Szewczenko, W. Walke, K. Nowinska, J. Marciniak, Corrosion resistance of Ti-6Al-4V alloy after diverse surface treatments, Corrosion 41 (5) (2010) 360–371.
[16] A. El-ghannam, L. Starr, J. Jones, Laminin-5 coating enhances epithelial cell attachment spreading and hemidesmosome assembly on Ti-6Al-4V implant material in vitro, J. Biomed. Mater. Res. 41 (1) (1998) 30–40.
[17] D.G. Castner, B.D. Ratner, Biomedical surface science: foundations to frontiers, Surf. Sci. 500 (1–3) (2002) 28–60.
[18] B.D. Ratner, A history of biomaterials, in: B.D. Ratner, S. Hoffman A, S. FJ, L. JE (Eds.), Biomaterials Science: An Introduction to Materials in Medicine, second ediElsevier 2004, pp. 10–23.
[19] S.R. Paital, N.B. Dahotre, Calcium phosphate coatings for bio-implant applications: materials, performance factors, and methodologies, Mater. Sci. Eng. R. Rep. 66 (1–3) (2009) 1–70.
[20] C.M. Stanford, Surface modification of biomedical and dental implants and the processes of inflammation, wound healing and bone formation, Int. J. Mol. Sci. 11 (1) (2010) 354–369.
[21] J. Vaithilingam, S. Kilsby, R.D. Goodridge, S.D.R. Christie, S. Edmondson, R.J.M. Hague, Immobilisation of an antibacterial drug to Ti6Al4V components fabricated using selective laser melting, Appl. Surf. Sci. 314 (2014) 642–654.
[22] M. Kawase, T. Hayashi, M. Asakura, A. Mieki, H. Fuyamada, M. Sassa, et al., Cell proliferation ability of mouse fibroblast-like cells and osteoblast-like cells on a Ti-6Al-4V alloy film produced by selective laser melting, Mater. Sci. Appl. 5 (2014) 475–483.
[23] B.S. Van, Y.C. Chai, S. Truscello, M. Moesen, G. Kerckhofs, O.H. Van, et al., The effect of pore geometry on the in vitro biological behavior of human periosteum-derived cells seeded on selective laser-melted Ti6Al4V bone scaffolds, Acta Biomater. 8 (7) (2012) 2824–2834.

[24] J. Markhoff, J. Wieding, V. Weissmann, J. Pasold, A. Jonitz-heincke, R. Bader, Influence of different three-dimensional open porous titanium scaffold designs on human osteoblasts behavior in static and dynamic cell investigations, Materials (Basel) 8 (2015) 5490–5507.
[25] I. Gibson, D.W. Rosen, B. Stucker, Additive Manufacturing Technologies, Springer, US, 2010.
[26] F. Variola, J.-H. Yi, L. Richert, J.D. Wuest, F. Rosei, A. Nanci, Tailoring the surface properties of Ti6Al4V by controlled chemical oxidation, Biomaterials 29 (10) (2008) 1285–1298.
[27] M. Ask, J. Lausmaa, B. Kasemo, Preparation and surface spectroscopic characterization of oxide films on Ti6Al4V, Appl. Surf. Sci. 35 (3) (1989) 283–301.
[28] B. Vandenbroucke, J.-P. Kruth, Selective laser melting of biocompatible metals for rapid manufacturing of medical parts, Rapid Prototyp. J. 13 (4) (2007) 196–203.
[29] I. Yadroitsev, I. Smurov, Surface morphology in selective laser melting of metal powders, Phys. Procedia 12 (2011) 264–270.
[30] H. Zreiqat, S.M. Valenzuela, B.B. Nissan, R. Roest, C. Knabe, R.J. Radlanski, et al., The effect of surface chemistry modification of titanium alloy on signalling pathways in human osteoblasts, Biomaterials 26 (36) (2005) 7579–7586.
[31] Y. Fu, H. Du, S. Zhang, W. Huang, XPS characterization of surface and interfacial structure of sputtered TiNi films on Si substrate, Mater. Sci. Eng. A 403 (1–2) (2005) 25–31.
[32] A.P. Dementjev, G.A. De, S.M.C.M. Van De, K.I. Maslakov, X-ray photoelectron spectroscopy reference data for identification of the C3 N4 phase in carbon-nitrogen films, Diam. Relat. Mater. 9 (2000) 1904–1907.
[33] M. Rombouts, J.P. Kruth, L. Froyen, P. Mercelis, Fundamentals of selective laser melting of alloyed steel powders, CIRP Ann. Manuf. Technol. 55 (1) (2006) 187–192.
[34] C. Leyens, Oxidation and protection of titanium alloys and titanium aluminides, in: M. Peters, C. Leyens (Eds.), Titan. Titan. Alloy, Wiley-Vch Verlag GmbH & Co. 2003, pp. 187–223.
[35] M.D. Hamilton, Anatase phase, hydrophilicity, and thickness of thermally oxidized TiO2 layer on titanium-V alloy, J. Undergrad. Res. 6 (2013) 16–19.
[36] A. Pequegnat, A. Michael, J. Wang, K. Lian, Y. Zhou, M.I. Khan, Surface characterizations of laser modified biomedical grade NiTi shape memory alloys, Mater. Sci. Eng. C 50 (2015) 367–378.
[37] S. Axelsson, Surface Characterization of Titanium Powders with X-ray Photoelectron Spectroscopy [Diploma Thesis], 2012 Available from: http://publications.lib.chalmers.se/records/fulltext/164534.pdf.
[38] D. Devilliers, M.T. Dinh, D. Krulic, N. Larabi, N. Fatouros, Behaviour of titanium in sulphuric acid: application to DSAs, J. New Mater. Electrochem. Syst. 232 (2006) 221–232.
[39] H. Kim, S.-H. Choi, J.-J. Ryu, S.-Y. Koh, J.-H. Park, I.-S. Lee, The biocompatibility of SLA-treated titanium implants, Biomed. Mater. 3 (2) (2008) 1–6.
[40] J. Vaithilingam, R.D. Goodridge, R.J.M. Hague, S.D.R. Christie, S. Edmondson, The effect of laser remelting on the surface chemistry of Ti6al4V components fabricated by selective laser melting, J. Mater. Process. Technol. 232 (2016) 1–8.
[41] Y.-T. Sul, Electrochemical growth behavior, surface properties, and enhanced in vivo bone response of TiO2 nanotubes on microstructured surfaces of blasted, screw-shaped titanium implants, Int. J. Nanomedicine 5 (2010) 87–100.
[42] C.A. Scotchford, G. CP, E. Cooper, L. GJ, S. Downes, Protein adsorption and human osteoblast-like cell attachment and growth on alkylthiol on gold self-assembled monolayers, J. Biomed. Mater. Res. 59 (1) (2002) 84–99.
[43] J. Vaithilingam, S. Kilsby, R.D. Goodridge, S.D.R. Christie, S. Edmondson, R.J.M. Hague, Functionalisation of Ti6Al4V components fabricated using selective laser melting with a bioactive compound, Mater. Sci. Eng. C 46 (2015) 52–61.
[44] J. Matena, S. Petersen, M. Gieseke, A. Kampmann, M. Teske, M. Beyerbach, et al., SLM produced porous titanium implant improvements for enhanced vascularization and osteoblast seeding, Int. J. Mol. Sci. 16 (2015) 7478–7492.